Fast in situ 3D nanoimaging: a new tool for dynamic characterization in materials science

Julie Villanova, Rémi Daudin, Pierre Lhuissier, David Jauffres, Siyu Lou, Christophe L. Martin, Sylvain Labouré, Rémi Tucoulou, Gema Martinez-Criado, Luc Salvo

Fast *in situ* 3D nanoimaging: a new tool for dynamic characterization in materials science

Julie Villanova[1,*], Rémi Daudin[2], Pierre Lhuissier[2], David Jauffrès[2], Siyu Lou[2], Christophe L. Martin[2], Sylvain Labouré[1], Rémi Tucoulou[1], Gema Martínez-Criado[1,3] and Luc Salvo[2]

[1] ESRF The European Synchrotron, CS 40220, 38043 Grenoble Cedex 9, France
[2] University Grenoble Alpes, CNRS, SIMaP, F-38000 Grenoble, France
[3] Instituto de Ciencia de Materiales de Madrid, Consejo Superior de Investigaciones Científicas, 28049 Cantoblanco, Spain

The performance of many advanced materials is determined by the arrangement of their nanostructure which requires ever more precise characterization. In this respect, X-ray computed tomography (CT) is a powerful technique to investigate material properties as it provides non-destructive direct access to three-dimensional morphology with nanoscale resolution. However, challenges remain in clearly understanding physical mechanisms involved during their processing in real time and real conditions. So far, beam and sample stabilities, effective spatial resolution and tomography scan time have hindered the development of nanoscale *in situ* 4D imaging (3D plus time), and especially at high temperatures. Here, we report on the development of fast X-ray nanotomography at temperatures up to 700°C with an unprecedented combination of nanometer pixel size and acquisition times of a few tens of seconds. The great potential of the method is demonstrated by following the early stages of two thermally driven phenomena: neck curvature evolution in sintering and nucleation of liquid droplets in light alloys. The reported real time observations will benefit the fundamental understanding of the underlying physics and provide useful data to build new models. The novel aspects of this synchrotron based technique offer a powerful imaging tool for a wide variety of heterogeneous nanoscale dynamics in materials and open new perspectives for the investigation of advanced materials under realistic conditions.

Introduction

X-ray computed tomography (CT) is an effective imaging tool that has found broad applications in medicine, biology but also in materials science and nanoscience [1–4]. Indeed, 3D characterization is an efficient approach to tackle effective properties that are dictated by 3D phase morphology [5,6]. Using different contrast mechanisms (e.g. absorption, phase, diffraction, scattering), a three-dimensional (3D) representation of the sample is reconstructed from two-dimensional (2D) projections recorded at different angles. Today, a wide spectrum of length scales can be probed, ranging from a few micrometers on millimeter-sized objects to tens of nanometers on micrometer-sized samples, using lab-scale equipment or synchrotron sources [7,8]. Because images are collected non-destructively, the technique can be applied repeatedly to follow material structural changes in real time [9,10]. Thus, processes that occur over a wide range of timescales have been studied with series of 3D images often called '4D' imaging. For example, at micrometer length scales, entire plant life cycles that typically take place over weeks or months have been studied using laboratory instruments [11], whereas faster events such as live flying insects within sub-millisecond frame rates have been followed at synchrotron sources [12]. *In situ* observations (e.g. heating, cooling and deformation) are currently achievable with micrometer spatial resolution in the hard X-ray domain. Some

*Corresponding author: Villanova, J. (julie.villanova@esrf.fr)

examples include failure mechanisms of ceramic matrix composites operating under load at high temperatures [4], lithiation dynamics under current reduction [10], topological symmetry breaking in viscous coarsening [13], and cellular solidification of colloidal suspensions [14].

Despite these notable achievements and the development of new set-ups such as nanoscale zoom tomography by Mokso et al. [15], the combination of real time, *in situ* and CT in the nanometer regime remains a key challenge. CT studies at high temperatures generally address materials damage, deformation and growth mechanisms, as well as remelting, solidification and sintering. However, the early stages of many of these phenomena (e.g. growth kinetics, nucleation of phases or cracks) demand 4D examination at the nanoscale. So far, one of the major limitations is the compromise that has to be made between two critical parameters: pixel size (related to the resulting spatial resolution), and time required to fully acquire a 3D image (tomography scan time). Since the early 90s, there has been a gradual improvement thanks to the higher photon flux provided by synchrotron sources and faster CMOS detector technology. These developments are summarized in Fig. 1, which shows the achieved pixel size against scan time for more than 240 *in situ* CT experiments from the literature (between 1995 and 2017, see http://tinyurl.com/Fast-Tomography for a full references list and Figs 2S and 3S for more information) at room and high temperatures. Figure 1 reveals that high spatial resolution (nanometer) and rapid scan rates (tens of seconds) have been so far mutually exclusive for *in situ* observations, surely because of a lack of mechanical reliability, inferior detection speed and not accurate enough temperature stability. The *in situ* 4D imaging tool presented here overcome all these limitations, allowing a significant step forward in terms of scan time and pixel size.

Fast *in situ* X-ray nanotomography at high temperature

Figure 2 shows the schematic layout of our experimental arrangement, which utilizes the hard X-ray nanotomography set-up

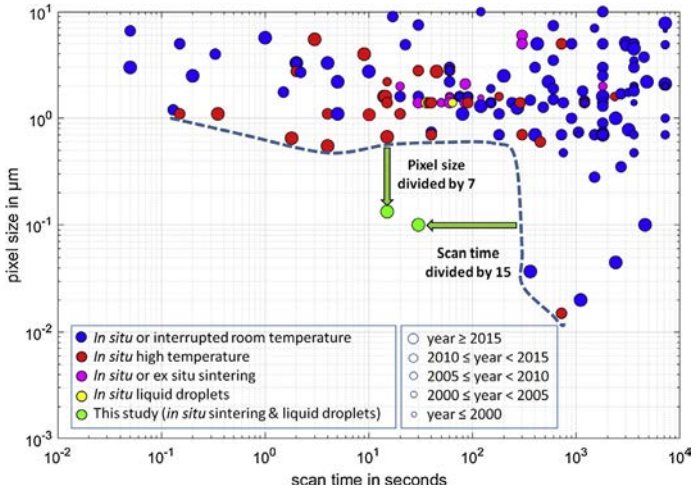

FIGURE 1

State of the art of *in situ* X-ray tomography: Pixel size *versus* scan time illustrating the state of the art for *in situ* X-ray laboratory and synchrotron tomography. Scan times of about 10 min are usually necessary to operate with nanometer pixel size (≤100 nm). Similarly, ultra-fast tomography (≤10 s time scan) is only attainable with micrometer resolution. The database on which this figure is based, is available at: http://tinyurl.com/Fast-Tomography.

developed at the nano-probe beamline ID16B at the European Synchrotron Radiation Facility (ESRF) [16,17]. Speed and stability are crucial prerequisites to implement 3D acquisitions at high temperatures. On the basis of magnified phase contrast, an intense hard X-ray nanobeam (50 nm × 50 nm spot size with 10^{12} ph/s) combined with a PCO edge 5.5 detector (equipped with a CMOS sensor) facilitates fast acquisitions with a high dynamic range (16 bit). Single distance acquisition is essential for 4D since time is not available to move the sample to different distances. The single distance phase retrieval method is detailed in the section 'Image reconstruction'. To meet our demanding specifications, a customized high temperature heating solution was build. With a rapid heat-up rate, the robust bottom loading furnace is based on a MHI FibHeat200-XRD microheater allowing temperatures as high as 1000°C to be reached. Several modifications on the microheater have been necessary to minimize and control the thermal drift of the sample and to attain the stability required at the nanoscale. An efficient water cooling system (Fig. 2) protects the thermally regulated experimental hutch (±0.05°C) [17] from significant temperature variation (more details on the tomography acquisition and set-up are provided in Supplementary Information).

The set-up allows high temperature CT scans to be performed in 20 s with a pixel size of about 100 nm. These performances are nearly one order of magnitude lower in pixel size and 15 times faster than all other currently available CT schemes. We used this real time *in situ* X-ray nanotomography system to study two phenomena at high temperatures: the neck size and curvature evolution during the early stages of sintering of glass particles, and the nucleation of liquid droplets in Aluminum–Copper (Al–Cu) alloys.

Sintering of ceramic materials

The understanding and modeling of the sintering stages of metals and ceramic/glass materials is crucial to process defect-free bulk systems or structures with controlled porosity [18]. CT has played a

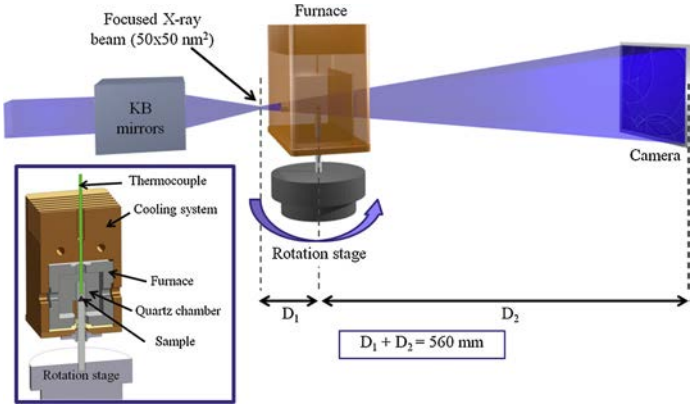

FIGURE 2

Schematic layout of *in situ* 4D nano-imaging set-up: X-rays are focused down to a spot size of 50 nm × 50 nm using two multilayer-coated Si mirrors in Kirkpatrick–Baez (KB) configuration under pink beam mode. The sample located in the microheater is positioned out of the focal plane in projection geometry. While rotating the sample over 360°, high-resolution images are collected by a PCO camera. Pixel size and field of view of the scans depend on the sample position between the focal plane and the detector which are at a fixed distance of each other such as $D_1 + D_2 = 560$ mm (see Supplementary Information). The inset shows a close-up of the microheater, revealing key components: cooling system, furnace, quartz chamber and thermocouple.

key role to follow the densification of both metallic [19–22] and glass powders [23,24]. However, owing to the limited spatial resolution, previous experiments were performed at the scale of several hundreds of particles, thus focusing on rearrangement phenomena, neck growth, pore growth or strain anisotropy. The pixel sizes, ranging from 1.4 to 5 μm, did not allow the visualization of the early stages of sintering or a quantitative assessment of the neck curvature [19], which is a key parameter governing sintering [25]. Many models are based on the so-called tangent-circle approximation, assuming a constant neck curvature [25,26], whereas FEM [27] or optical micrographs [28] clearly show that this hypothesis is too idealistic. No precise measurements have been reported so far on a real *in situ* sintering system. Here, we present for the first time an estimation of the neck curvature evolution at the early stages of a sintering process using real time *in situ* nanotomography.

Spherical soda-lime glass particles were isothermally treated at 670°C, and a total of 90 tomography scans (33 s each) were recorded during one hour and 45 min. With a pixel size of 100 nm (see Supplementary Information for scan details), the initial and intermediate stages of the sintering were examined. The growth of necks down to a few microns in size was accurately followed as shown in Fig. 3. Two types of necks can be distinguished: large ones (I and II) that originate from contacts that are initially present, and smaller ones (III and IV) formed during the early stage of sintering [24]. The growth curve of neck II exhibits an inflexion point around 50 min related to its coalescence with neck I, thus slowing down its growth. The classical Frenkel two sphere viscous sintering model [29], which predicts a neck size that scales with the square root of time, is not able to reproduce our data. In this temperature range, glass sintering probably mainly occurs via viscous flow but other mechanisms such as viscoelastic sintering or non-Newtonian viscous flow cannot be excluded and may explain this departure [24]. Also, Frenkel's model was previously experimentally supported only by *in situ* optical microscopy with very specific 1D or 2D particle configurations [28,30] in which 3D particle rearrangement and neck impingement phenomena are

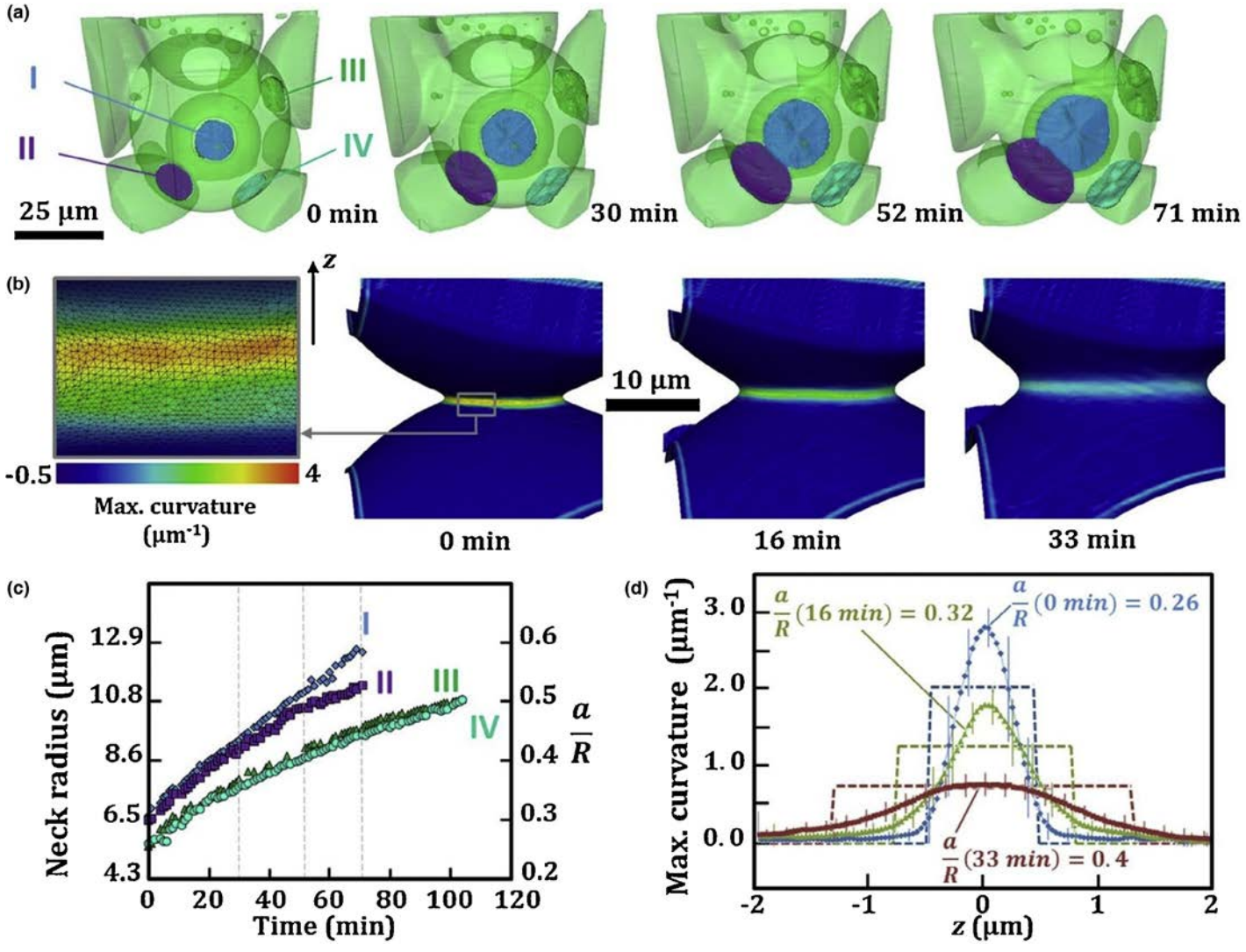

FIGURE 3

In situ X-ray nanotomography of glass particles sintering at 670°C. (a) 3D rendering of the investigated volume showing the growth of four segmented necks (I–IV). (b) Neck IV surface mesh displaying maximum principal curvature. (c) Neck radius *versus* time. *a*/*R* refers to the relative neck radius (neck radius: *a*, particle radius: *R*). The dashed vertical lines correspond to the 3D images in (a). (d) Comparison between experimental maximum principal curvature (symbols) and the tangent-circle approximation (dashed lines) as a function of the distance *z* from the neck plane.

unrealistically limited. Our observations of real 3D packings reveal some limitations of early models to mimic a real system with multiple interacting particles in 3D. Thanks to the high resolution provided by our *in situ* 4D imaging approach, neck curvatures can also be extracted from surface meshing (Fig. 3b). Neck IV has been selected to estimate the curvature. After averaging in the vicinity of planes parallel to the neck plane, the local curvature is compared to the tangent-circle approximation in Fig. 3d. The Coble geometrical model of the neck [26] suggests that the neck geometry can be approximated by an inverted tore tangent to the spherical particles while obeying volume conservation. Our finding, based on 3D experimental observations, demonstrates that the constant curvature hypothesis, although useful to build densification models [25,26,29], is an invalid assumption. The investigated neck clearly displays a more pronounced curvature and a reduced thickness compared to the basic tangent-circle approximation. In brief, the availability of data with nanometer resolution on real 3D systems allows the reassessment of two-sphere models and provides a reliable foundation for further sophisticated models, which will give access to a better understanding of the influence of local packing on the development of sintering defects.

Remelting of light metal alloys, new insight for additive manufacturing

Light metal alloys, such as magnesium or aluminum based alloys, respond to the major challenge of lighter and stronger materials for transportation and energy saving applications. Whereas alloy solidification has been extensively studied, the development of

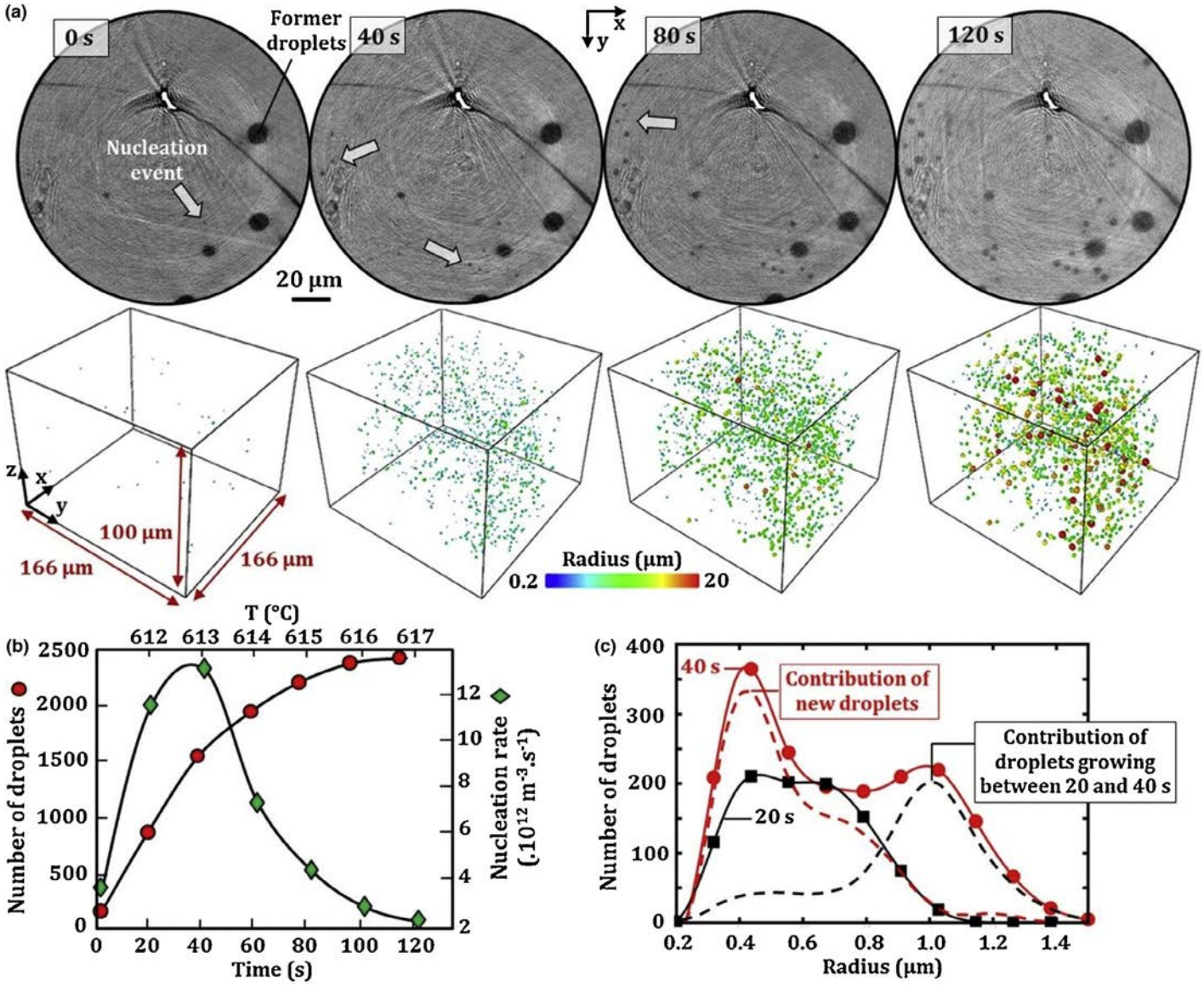

FIGURE 4

In situ investigation of liquid droplet nucleation: (a) 2D slices extracted from the 3D images at 0, 40, 80 and 120 s, and 3D visualization of the location, number and size of nucleating droplets during remelting of the Al–2.6 wt.% Cu sample. (b) Evolution of the number of droplets (red-dot) and nucleation rate (green-diamond) with time and temperature deduced from the 3D quantitative analysis. (c) Radius distribution of the liquid droplets at 20 s (plain black-square) and 40 s (plain red-dot). Dashed lines were obtained by performing the radius distribution analysis at 40 s on the liquid droplets nucleating at this stage only (dashed red), and on the liquid droplets that were already present at 20 s only (dashed black), demonstrating the contribution of each population to the overall bi-modal distribution.

new additive manufacturing techniques involving powder melting, like SLM or EBM [31], requires fresh insights into remelting phenomena. Some particles are only partially remelted while others undergo full melting. During the partial remelting of alloys, liquid droplets are formed [32–34]. This liquid nucleation in a solid state has been observed only recently using *in situ* CT by Terzi et al. (yellow points, Fig. 1) [35]. A subsequent 4D imaging work, which investigated in more detail the internal melting and coarsening of liquid droplets in an Al–Cu alloy [36], did not allow the nucleation of droplets to be visualized due to the 1.4 μm pixel size. Using high-resolution scanning electron microscopy, by contrast, the nucleation step of liquid droplets has recently been observed in Al–Cu alloys. The samples were partially remelted and then quenched to track frozen droplets smaller than 100 nm [37]. The quantitative analysis of 2D post mortem images via growth models yields an estimation of the nucleation rate of liquid droplets between 10^{13} and 10^{15} m^{-3} s^{-1}. Although this work provides insights into liquid nucleation, questions still remain because possible 3D microstructural changes may potentially occur during quenching [38]. To overcome the problems raised by these two early studies, here we use fast *in situ* nanotomography to investigate liquid droplet nucleation with a pixel size of 133 nm. The Al–Cu sample was solutionized for two hours at 540°C and reheated at 3°C/min in the semi-solid range up to 625°C. During the heating step, scans of 20 s with 800 projections were continuously acquired, leading to a total of 60 scans recorded in 20 min. Figure 4a displays 2D slices extracted from the reconstructed 3D images, where nucleation events were clearly detected during the sample heating. The whole set of 3D images was segmented to obtain a 3D rendering of the nucleation of the liquid droplets and to perform quantitative measurements (large droplets that were already present in the material before *in situ* measurements have been discarded). Figure 4b represents the evolution of the nucleation rate and the number of liquid droplets against time, while Fig. 4c shows droplet size distribution at 20 and 40 s. The estimated nucleation rate of about 10^{13} m^{-3} s^{-1} is within the range of the values determined on quenched samples [37]. As indicated in Fig. 4c, a double peak is observed in the droplet size distribution at 40 s. Taking advantage of the *in situ* capability, the droplets are fully tracked from 20 to 40 s. Our analysis reveals that the second peak in the size distribution is a consequence of the growth of existing droplets between the two scans, and not of the nucleation of new droplets. The new droplets in the scan at 40 s, which nucleate 20 s after the first scan, exhibit a radius in the range 0.3–0.5 μm. This finding is strikingly similar to that observed in the scan at 20 s, as well as in the following scans, thus revealing a 'critical' nucleation size available at our spatial resolution. It has also been determined that the bi-modal distribution is due to different growth rate linked to droplets neighboring. Thanks to the *in situ* tracking of the nucleation of such droplets with fast acquisition time, we observed a heterogeneous nucleation with specific arrangement maybe due to inhomogeneous solute distribution. Further fast *in situ* 3D investigations will help to clarify the unsolved question: is liquid droplet nucleation homogeneous or heterogeneous?

Conclusion

In conclusion, we have developed fast *in situ* synchrotron nanotomography and performed first real time measurements of thermally driven phenomena with unprecedented pixel size and acquisition time. We have obtained new results on two important phenomena in material processing (sintering and remelting) that pave the way for a better fundamental understanding of the underlying physics. Other potential applications include nucleation and growth of pores and cracks, glass synthesis, high temperature mineralization processes, mechanical integrity of catalyst materials, among others. We are now focused on extending the technique demonstrated here to very high temperature (above 1000°C) and in parallel pushing even further the spatial resolution. As advanced developments such as diffraction limited storage rings, X-ray nanofocusing optics, fast and large detectors are at present making rapid progress worldwide, real time *in situ* 4D nanoimaging can be further improved, capturing faster heterogeneous dynamics at multiple length scales. We thus anticipate that the experimental approach reported here will find broad applications across many fields in materials science.

Acknowledgments

We are grateful to the invaluable support from technical services of the ESRF. In particular, Cyril Guilloud and Roberto Homs for their useful help. We also thank the ESRF for the beamtime allocated. GMC thanks the partial financial support from CSIC through the project 201660I001. We would like to thank Franck Pelloux, Xavier Bataillon and Charles Josserond for their technical support.

Appendix A. Experimental section

Samples preparation and materials

For the sintering experiment, soda-lime glass spherical particles (composition 72.5 wt.% SiO_2, 13.7 wt.% Na_2O, 9.8 wt.% CaO, 3.3 wt.% MgO, 0.4 wt.% Al_2O_3, 0.1 wt.% K_2O) were poured in a quartz capillary (inner diameter: 100 μm, walls thickness: 10 μm). The capillary was glued on top of an alumina tube attached to the nanotomography sample holder.

For the liquid droplet nucleation experiment, an Al–Cu alloy of composition 2.6 wt.% Cu was used. The sample was machined in a cone shape to obtain a section thin enough for X-ray nanotomography and then glued to the top of an alumina tube as previously described.

Image reconstruction

Data processing consisted in a single distance phase retrieval calculation and 3D reconstruction. The phase retrieval calculation based on a Paganin-like [39] approach was performed using a homogenous δ/β ratio equal to 365 and 156 for glass particles and Al–Cu alloy respectively. A recursive calculation based on a non-linear conjugate gradient method [40,41], with ten iterations and assuming that the amplitude is set to the Paganin amplitude was subsequently applied to iteratively improve the phase estimation and increase the image quality. A specific padding scheme adapted to local tomography was used [42]. Phase retrieval was performed using an in-house software in the GNU Octave programming environment and the public domain image analysis program ImageJ [43]. Tomographic reconstruction using filtered phase maps was executed using backprojection with the ESRF software PyHST2 [44] (more details on the phase retrieval calculation are provided in Supplementary Information).

Image analysis

The segmentation of glass particles was performed using the ImageJ software following established procedures [22]. The procedure to assess local curvatures uses a mesh constructed on an isocontour of the grayscale reconstruction. The mesh is then treated using Avizo software to compute and visualize the curvatures. Segmentation of the liquid droplet forming within the Al–Cu alloy was carried out manually with Avizo to preserve small droplets from being erased systematically when using automatic filtering and thresholding.

References

[1] E. Maire, P.J. Withers, Int. Mater. Rev. 59 (2014) 1–43.
[2] K.J. Harry, et al. Nat. Mater. 13 (2014) 69–73.
[3] M. Ebner, et al. Science 342 (2013) 716–720.
[4] H.A. Bale, et al. Nat. Mater. 12 (2013) 40–46.
[5] G. Möbus, B.J. Inkson, Mater. Today 10 (2) (2007) 18–25.
[6] D. Van Gough, A.T. Juhl, P.V. Braun, Mater. Today 12 (6) (2009) 28–35.
[7] M. Scheel, et al. Nat. Mater. 7 (2008) 189–193.
[8] P.J. Withers, Mater. Today 10 (12) (2007) 26–34.
[9] D. Juul Jensen, et al. Mater. Today 9 (2006) 18–25.
[10] C. Villevieille, et al. Adv. Mater. 27 (2015) 1676–1681.
[11] S. Ahmed, et al. Plant Soil 401 (2016) 125–134.
[12] S.M. Walker, et al. PLoS Biol. 12 (2014) e1001823.
[13] D. Bouttes, E. Gouillart, D. Vandembroucq, Phys. Rev. Lett. 117 (2016) 145702.
[14] S. Deville, et al. Nat. Mater. 8 (2009) 966–972.
[15] R. Mokso, et al. Appl. Phys. Lett. 90 (2007) 144104.
[16] J. Villanova, et al. J. Mater. Sci. 49 (2014) 5626–5634.
[17] G. Martínez-Criado, et al. J. Synchrotron Radiat. 23 (2016) 344–352.
[18] Z. Yan, et al. Appl. Phys. Lett. 102 (2013) 223107.
[19] A. Vagnon, et al. Acta Mater. 56 (2008) 1084–1093.
[20] O. Lame, et al. Acta Mater. 52 (2004) 977–984.
[21] L. Olmos, et al. J. Mater. Sci. 49 (2014) 4225–4235.
[22] R. Grupp, et al. Nat. Commun. 2 (2011) 298.
[23] D. Bernard, et al. Acta Mater. 59 (2011) 6228–6238.
[24] D. Bernard, et al. Acta Mater. 53 (2005) 121–128.
[25] R.M. German, Sintering: From Empirical Observations to Scientific Principles, Butterworth-Heinemann, 2014.
[26] R.L. Coble, J. Am. Ceram. Soc. 41 (1958) 55–62.
[27] F. Wakai, et al. Acta Mater. 109 (2016) 292–299.
[28] H.E. Exner, G. Petzow, in: G.C. Kuczynski (Ed.), Shrinkage and Rearrangement During Sintering of Glass Spheres in Sinter. Catal., Springer US, 1975, pp. 279–293.
[29] J. Frenkel, J. Phys. 9 (1945) 385–391.
[30] M. Godinho, et al. J. Chem. Educ. 83 (2006) 410.
[31] W.E. Frazier, J. Mater. Eng. Perform. 23 (2014) 1917–1928.
[32] S. Annavarapu, R.D. Doherty, Acta Metall. Mater. 43 (1995) 3207–3230.
[33] F. Czerwinski, A. Zielinska-Lipiec, Acta Mater. 51 (2003) 3319–3332.
[34] S. Kleiner, O. Beffort, P.J. Uggowitzer, Scr. Mater. 51 (2004) 405–410.
[35] S. Terzi, et al. Scr. Mater. 60 (2009) 671–674.
[36] S. Terzi, et al. J. Mater. Sci. 48 (2013) 7422–7434.
[37] S. Lippmann, M. Fink, M. Rettenmayr, Acta Mater. 72 (2014) 32–40.
[38] O. Pompe, M. Rettenmayr, J. Cryst. Growth 192 (1998) 300–306.
[39] D.M. Paganin, Coherent X-Ray Optics, vol. 6 of Oxford Series on Synchrotron Radiation, Oxford University Press, Oxford, 2006.
[40] L. Weber, Iterative Tomographic X-Ray Phase Reconstruction, (Ph.D. thesis), September 2016.
[41] M. Langer, et al. PLoS ONE 7 (2012) e35691.
[42] J. Villanova, et al. J. Power Sources 243 (2013) 841–849.
[43] P. Cloetens, et al. Appl. Phys. Lett. 75 (1999) 2912.
[44] A. Mirone, et al. Nucl. Instrum. Methods B 324 (2014) 41–48.